Meas. Sci. Technol. **19** (2008) 015408 (9pp) doi:10.1088/0957-0233/19/1/015408

The scanning flow cytometer modified for measurement of two-dimensional light-scattering pattern of individual particles

Gleb V Dyatlov[1,3], Konstantin V Gilev[1], Konstantin A Semyanov[2] and Valeri P Maltsev[2,3,4]

[1] Sobolev Institute of Mathematics, Koptyug Avenue 4, Novosibirsk 630090, Russia
[2] Institute of Chemical Kinetics and Combustion, Institutskaya 3, Novosibirsk 630090, Russia
[3] Novosibirsk State University, Pirogova 2, Novosibirsk 630090, Russia
[4] State Research Center of Virology and Biotechnology 'VECTOR', Koltsovo, Novosibirsk Region 630559, Russia

E-mail: maltsev@kinetics.nsc.ru

Received 19 June 2007, in final form 7 November 2007
Published 17 December 2007
Online at stacks.iop.org/MST/19/015408

Abstract
We theoretically consider a new approach for measurement of the two-dimensional light-scattering patterns (2D LSP) of individual particles (for example, blood cells). Unlike the original optical scheme of the scanning flow cytometer that integrates scattering intensity over the azimuth angle, the new scheme allows us to measure the 2D LSP. The approach assumes measurement of the integral distribution of intensity on the fixed plane with subsequent reconstruction of the pattern via solving a first-kind integral equation. The last problem is ill-posed and we solve this equation by the standard regularization method. Error sources of the new approach are discussed from a comparison of the initial and reconstructed 2D LSPs for non-spherical particles.

Keywords: optical instrumentation, integral equation, inverse problem, non-spherical particle light scattering, scanning flow cytometer

1. Introduction

The approach to studying small particles based on reconstruction of particle parameters from their scattering properties plays an important role in various fields of science and technology. This approach assumes mathematical modeling of the electromagnetic scattering process. Then we can solve the direct problem for a sufficiently large number of different particles and try to decide whose scattering data most likely correspond to the experimental data. Observe that the direct electromagnetic scattering problem is studied rather completely both theoretically and numerically [1–4].

Alternatively, we can try to solve immediately the inverse problem, i.e., to reconstruct the form and other properties of particles from the scattering data. However, this approach faces serious theoretical difficulties and, in spite of a large number of publications, the theory of inverse electromagnetic scattering is far from being complete [5–9].

Dealing with small particles such as blood cells, alongside purely theoretical issues related to solution of the inverse problem, we also face the practical problem of measurement of the light scattering caused by difficulties with particle localization and low light-scattering intensity from individual particles. The most efficient solution of the last problem supports a hydro- or aero-focusing technique that provides 5 μm localization of a particle within a laminar flow [4, 10, 11]. The other problem relates to sufficiency of experimentally measured data to provide good precision for the inversion algorithm. Ordinary instruments which measure light-scattering intensities at a few spatial angles do not solve this problem. Much more light-scattering information can be retrieved from the two-dimensional light-scattering pattern

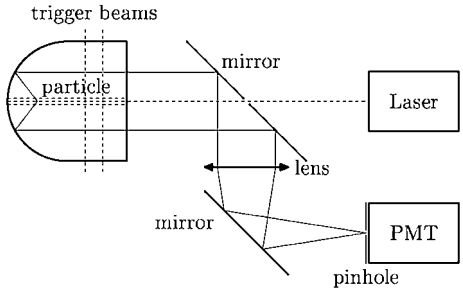

Figure 1. Original scanning scheme.

(2D LSP) that is the angular distribution of the light-scattering intensity in the polar and azimuth angles. Instrumentally this problem was solved for airborne particles [8] and water suspensions [12]. Unfortunately the instruments utilize rather expensive and unique equipment like an intensified CCD camera and an ellipsoidal mirror.

About a decade ago, we designed the scanning flow cytometer that allows us to measure the polar-angle distribution of the light-scattering intensity of individual particles [13]. This device makes it possible to collect rather rich information on the light scattering of small particles at a rate up to 500 particles s^{-1}. Mathematically, the measured function $s_{\text{int}}(\theta)$ is derived from integration of the 2D LSP $s(\theta, \varphi)$ over the azimuth angle φ, where $\theta \in [0, \pi]$, $\varphi \in [0, 2\pi]$, the incident light direction corresponds to $\theta = 0$, and the angle θ varies from 5° to 100° (see details in [7]). This information suffices for studying spherically symmetric particles, since $s(\theta, \varphi)$ is independent of φ in this case.

In the general case we wish to have the 2D LSP $s(\theta, \varphi)$ itself for the possibly widest range of angles. In this paper, we propose a modification of the scanning flow cytometer and also develop the corresponding mathematics.

2. Instrumental details

2.1. The original scanning scheme

For completeness of exposition, we will briefly describe the original scanning scheme (see figure 1). The detailed presentation can be found in [7]. The basic element of the scheme is the optical cuvette that is a quartz capillary with one flat and one spherical end. The water flow with particles goes into the cuvette from the left end. Positioning of the particle is carried out by means of two trigger laser beams. The laser beam (from Laser) is scattered by the particle flowing through the capillary. The scattered light reflected from the spherical end is focused by the mirror–lens–mirror unit and then reaches the pinhole with the photomultiplier tube (PMT) behind it. The device is designed so that the PMT measures only those rays which are parallel to the optical axis after reflection from the spherical end.

The mathematical description requires some notation. Let θ and φ be the polar and azimuth angles of the scattered ray. (The direction of the incident laser beam corresponds to $\theta = 0$.) Denote by $s(\theta, \varphi)$ the two-dimensional light-scattering pattern (2D LSP); i.e., for every pair (θ, φ) the value

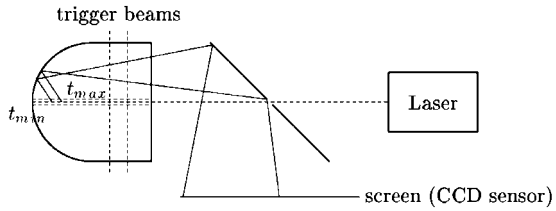

Figure 2. Modified scanning scheme. (Refraction is neglected.)

$s(\theta, \varphi)$ is the intensity of light scattered in the direction (θ, φ). The water flow is steady, and we can assume that $s(\theta, \varphi)$ does not change with time. For every position of the particle there is a unique value θ for which the rays with the polar angle θ are parallel to the optical axis after reflection from the spherical end and thereby reach the PMT. The particle moves along the capillary with constant speed; therefore, we have a one-to-one time-to-angle map (for details see [7]). Thus, we can measure the integral intensity

$$s_{\text{int}}(\theta) = \int_0^{2\pi} s(\theta, \varphi)\, \mathrm{d}\varphi.$$

On the one hand, integration over φ is caused by the construction of the scanner and is a disadvantage, since it leads to loss of information. On the other hand, the 2D LSP $s(\theta, \varphi)$ for an individual particle is very small, while the integral intensity $s_{\text{int}}(\theta)$ is large enough to be measured by the PMT at a rather high speed (about 1 MHz). In a sense, integration is a compulsory measure as we deal with small individual biological particles having slight light-scattering intensities. Moreover, in the case of spherical particles, $s(\theta, \varphi)$ is independent of φ and we lose no information.

2.2. The modified scanning scheme

Dealing with nonspherical particles such as red blood cells, it is desirable to have the complete 2D LSP $s(\theta, \varphi)$ for the possibly wider range of angles. It is natural to replace the lens–mirror–pinhole–PMT unit with a CCD sensor (see figure 2). However, here we face two main difficulties: the sensitivity and speed of widely available CCD sensors are insufficient for continuously measuring the 2D LSP of small individual particles. To overcome this complication, we propose to integrate; however, unlike the original scanning scheme, where we integrated with respect to the azimuth angle, now we integrate over some period of time.

Fix two particle positions t_{min} and t_{max} somewhere between the spherical bottom and the center of the sphere. We can identify these positions with time, for the flow speed is constant. We suppose that the flow is such that the particle does not change its orientation with time and remains in the exact center of the flow, for this assumption is in rather good agreement with experiment (see [14]). It means that the 2D LSP $s(\theta, \varphi)$ is the same at all times. We measure the intensity of light reaching the screen in the interval $[t_{\text{min}}, t_{\text{max}}]$, obtaining thereby the 'blurred' image of $s(\theta, \varphi)$. Denote by $\sigma(r, \psi)$ the density of the total light reaching the screen at the point with polar coordinates (r, ψ) during the indicated time interval. Below, we show that, under some additional

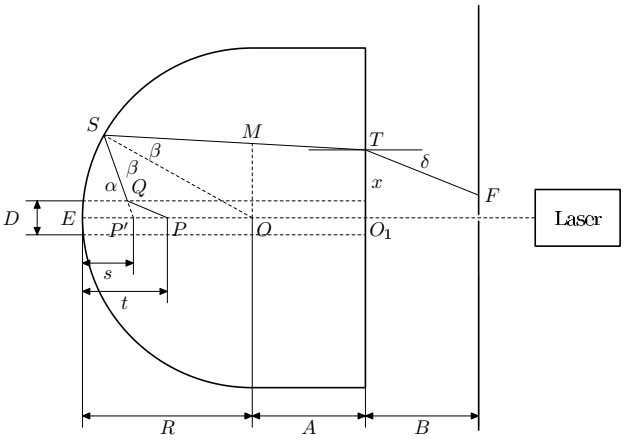

Figure 3. Optical scheme. R is the radius of the spherical end of the capillary ($R = 3$ mm); O is the center of the sphere; A is the distance from the center O to the right end of the capillary ($A = 2$ mm); B is the distance from the right end to the screen ($B = 3$ mm); D is the diameter of the capillary ($D = 254\ \mu$m); EO_1 is the optical axis; P is the position of the particle; Q is the point of refraction on the water–quartz interface; S is the point of reflection from the spherical end of the capillary; T is the point of refraction on the quartz–air interface; t is the distance from the particle to the left end E; F is the point at which the ray reaches the screen; M and P' are auxiliary points; s and x are auxiliary parameters.

constraints, $s(\theta, \varphi)$ and $\sigma(r, \psi)$ are connected by the integral relation

$$\int_0^{2\pi} K(r, \theta) s(\theta, \varphi) \mathrm{d}\theta = r\sigma(r, \varphi),$$

where the kernel $K(r, \theta)$ is determined by the optical scheme.

The goals of the paper are the following:

- find the integral dependence between $s(\theta, \varphi)$ and $\sigma(r, \psi)$;
- find out whether it is possible to reconstruct $s(\theta, \varphi)$ from $\sigma(r, \psi)$, in particular, for $\sigma(r, \psi)$ given with some error;
- justify the advisability of construction of the modified SFC.

3. Mathematics

3.1. Geometry of rays

The optical scheme of the modified scanner consists of a quartz capillary with one reflecting spherical and one flat end, a laser and a light-sensitive screen (CCD sensor) (see figure 3). For simplicity of computations, we assume that the screen is perpendicular to the optical axis as in figure 3. The light-scattering particle P lies in the cuvette on the optical axis at a distance t, $0 < t < R$, from the left end E.

Introduce the spherical coordinates (ρ, θ, φ) with center at the point P such that the direction of the incident laser beam corresponds to the polar angle $\theta = 0$. On the screen plane, we introduce the polar coordinates (r, φ) with center on the optical axis and such that the angle φ agrees with the azimuth angle φ of the spherical coordinate system. Consider the ray starting at P in the direction (θ, φ). After refraction on the water–quartz interface, reflection from the spherical end of the capillary, and refraction on the quartz–air interface, the ray reaches the screen at some point F. Since the refraction and reflection occur in the same plane, the φ-coordinate of F is equal to either φ or $\varphi + \pi$.

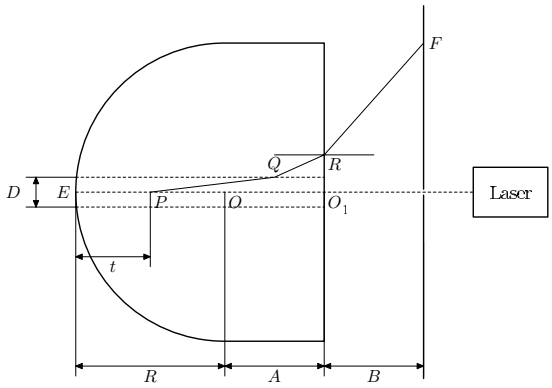

Figure 4. Backward rays.

Obviously, some rays may cross the optical axis, and hence rays with azimuth angles φ and $\varphi + \pi$ may come to the same point on the screen. To overcome this complication, from the very beginning we work with angles $\varphi \in [0, \pi]$, assuming that rays with other φ are eliminated by shading. With this assumption, it is convenient to use the modified polar coordinates in the screen plane:

$$x = r\cos\varphi, \quad y = r\sin\varphi, \quad r \in \mathbb{R}, \quad \varphi \in [0, \pi]. \tag{1}$$

In this case the ψ-coordinate of F is always equal to the parameter φ of the ray.

Besides the rays like PQSTF in figure 3, there are rays which go to the screen directly, without reflection from the spherical end of the capillary (see figure 4). We call them *backward rays*, because the polar angle θ of these rays is always greater than $\pi/2$. Since the pattern $s(\theta, \varphi)$ is small for θ close to π, the contribution of these rays is small and can be neglected.

3.2. Connection among t, θ and r

Naturally, we need the connection between the parameters t and θ of the ray and the coordinate r of the point F. Using the laws of refraction and reflection, we can write down the following system of equations (see figure 3):

$$\cos\alpha = \frac{n_\mathrm{w}}{n_\mathrm{q}}\cos\theta \quad \text{(the law of refraction at } Q\text{)} \tag{2}$$

$$t - s = \frac{D}{2}(\cot\theta - \cot\alpha) \quad \text{(from } \triangle PQP'\text{)} \tag{3}$$

$$R\sin\beta = (R - s)\sin\alpha \quad \text{(the sine theorem in } \triangle P'SO\text{)} \tag{4}$$

$$R\sin\beta = (x + A\tan(\alpha - 2\beta))\cos(\alpha - 2\beta) \quad \text{(the sine theorem in } \triangle SMO\text{)} \tag{5}$$

$$x - r = B\tan\delta \tag{6}$$

$$\sin\delta = \frac{n_\mathrm{q}}{n_0}\sin\gamma = \frac{n_\mathrm{q}}{n_0}\sin(\alpha - 2\beta) \quad \text{(the law of refraction at } T\text{)}. \tag{7}$$

The scheme imposes the following constraints on the ray parameters:

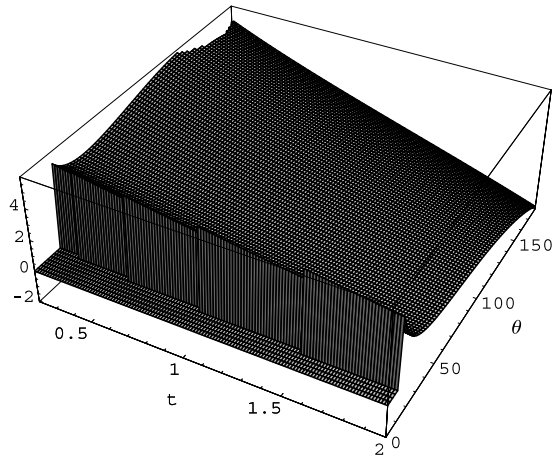

Figure 5. The function $r(\theta, t)$ for a wide range of t ($t \in [0.5, 2.2]$). The value $r(\theta, t)$ for nonadmissible (θ, t) is zero.

$$t \tan\theta > \frac{D}{2}, \qquad \frac{D}{2} < x < R,$$
$$(R - s)\sin\alpha > -R\cos\alpha. \tag{8}$$

The last condition means that the ray is reflected from the spherical end of the capillary. It holds automatically for $0 < \alpha < \pi/2$. Those pairs (θ, t) and triples (θ, t, r) for which the ray satisfies the above constraints are called *admissible*.

Obviously, the above equations make it possible to write down the dependence $r = r(\theta, t)$ explicitly; however, we do not do this in view of its bulkiness. This dependence (for admissible pairs (θ, t)) is shown in figure 5.

3.3. Connection between $s(\theta, \varphi)$ and $\sigma(r, \varphi)$

Knowing the geometry of rays, we can try to reconstruct the 2D LSP from the intensity of light on the screen.

Our problem is to reconstruct $s(\theta, \varphi)$ from $\sigma(r, \varphi)$.

Establish the dependence between these functions which is of integral character. Let $\rho(r, t, \varphi)$ be the light intensity on the screen (per unit area) at time t (i.e., the total intensity coming to the disk of radius r_0 centered at the origin during the interval $(t_{\min}, t_{\max})$ is equal to $\int_0^{2\pi}\int_0^{r_0}\int_{t_{\min}}^{t_{\max}} \rho(r, t, \varphi)\, r\,\mathrm{d}t\,\mathrm{d}r\,\mathrm{d}\varphi$).

Consider the (θ, t, φ)-space, the (r, t, φ)-space and the function $(\theta, t, \varphi) \mapsto (r(\theta, t), t, \varphi)$ from one space to the other. Take a domain U in the (θ, t, φ)-space; let V be its image in the (r, t, φ)-space; and suppose that the correspondence between them is one-to-one. As seen from figure 5, this is true, for example, if U is a convex set containing no points at which $r_\theta(\theta, t) = 0$. In this case, we also have the functions $t(\theta, r)$ and $\theta(r, t)$ on the corresponding two-dimensional domains. The derivation of the dependence between $s(\theta, \varphi)$ and $\sigma(r, \varphi)$ relies upon the fundamental fact that the total energy 'going from' U equals the total energy 'going to' the domain V:

$$\iiint_U s(\theta, \varphi)\sin\theta\,\mathrm{d}\theta\,\mathrm{d}t\,\mathrm{d}\varphi = \iiint_V \rho(r, t, \varphi) r\,\mathrm{d}r\,\mathrm{d}t\,\mathrm{d}\varphi. \tag{9}$$

Choose the domains U and V by means of the conditions $\theta_1 < \theta < \theta_2$, $r_1 < r < r_2$, and $\varphi_1 < \varphi < \varphi_2$; i.e.,

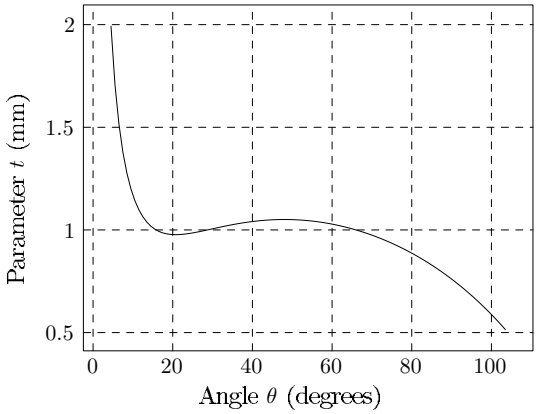

Figure 6. Typical dependence of t on θ for large r (here $r = 3.5$). The angle is counted in degrees.

$$U = \{(\theta, t, \varphi) \mid \theta_1 < \theta < \theta_2, t(\theta, r_2) < t < t(\theta, r_1), \varphi_1 < \varphi < \varphi_2\} \tag{10}$$

$$V = \{(r, t, \varphi) \mid r_1 < r < r_2, t(\theta_2, r) < t < t(\theta_1, r), \varphi_1 < \varphi < \varphi_2\}. \tag{11}$$

Note that the dependence $t(\theta, r)$ as a function of r for a fixed θ is always decreasing, while the same dependence as a function of θ for a fixed r has monotonicity intervals depending on r. In the definition of U and V above, we assumed that the latter function is decreasing (which is true for small r). We have

$$\int_{\varphi_1}^{\varphi_2}\int_{\theta_1}^{\theta_2}\int_{t(\theta,r_2)}^{t(\theta,r_1)} s(\theta, \varphi)\sin\theta\,\mathrm{d}t\,\mathrm{d}\theta\,\mathrm{d}\varphi = \int_{\varphi_1}^{\varphi_2}\int_{r_1}^{r_2}\int_{t(\theta_2,r)}^{t(\theta_1,r)} \rho(r, \varphi, t) r\,\mathrm{d}t\,\mathrm{d}r\,\mathrm{d}\varphi. \tag{12}$$

In view of the arbitrariness of φ_1 and φ_2, we can remove the integral with respect to φ. Calculate explicitly the integral with respect to t on the left-hand side and divide by $r_2 - r_1$:

$$\int_{\theta_1}^{\theta_2} \frac{t(\theta, r_1) - t(\theta, r_2)}{r_2 - r_1} s(\theta, \varphi)\sin\theta\,\mathrm{d}\theta = \frac{1}{r_2 - r_1}\int_{r_1}^{r_2}\int_{t(\theta_2,r)}^{t(\theta_1,r)} \rho(r, t, \varphi) r\,\mathrm{d}t\,\mathrm{d}r. \tag{13}$$

Letting r_2 tend to r_1, we obtain

$$-\int_{\theta_1}^{\theta_2} t_r(\theta, r_1) s(\theta, \varphi)\sin\theta\,\mathrm{d}\theta = \int_{t(\theta_2,r_1)}^{t(\theta_1,r_1)} \rho(r_1, t, \varphi) r_1\,\mathrm{d}t. \tag{14}$$

Numerical analysis shows that the correspondence $\theta \mapsto t(\theta, r)$ for a fixed r is univalent and is either monotone or has several local extrema θ_i (see figure 6).

Now, consider $\sigma(r, \varphi)$ for $r \in [r_{\min}, r_{\max}]$. Suppose that $t_{\min}$ and $t_{\max}$ are chosen so that, for all indicated r, $t_{\max}$ is greater than the local maximum (if any) and $t_{\min}$ is less than the local minimum (if any). Then we can uniquely determined the inverse images $\theta_{\min}(r)$ and $\theta_{\max}(r)$ of the points $t_{\max}$ and $t_{\min}$ under the mapping $t(\theta, r)$. Split, if needed, the interval $[\theta_{\min}(r), \theta_{\max}(r)]$ into the monotonicity intervals and note

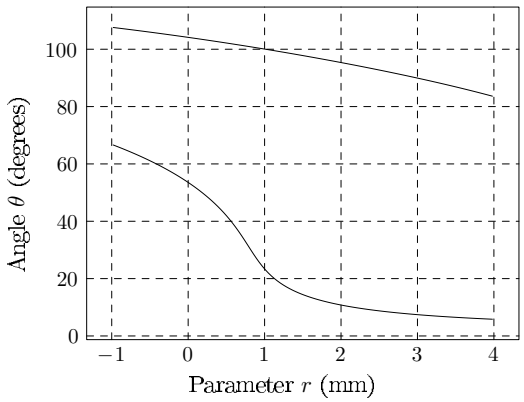

Figure 7. The functions $\theta_{\min}(r)$ and $\theta_{\max}(r)$ for $t_{\min} = 0.8$ and $t_{\max} = 1.5$.

that in the case of several monotonicity intervals $\sigma(r, \varphi)$ is composed of the integrals of $\rho(r, t, \varphi)$ over overlapping time intervals; this situation corresponds to simultaneous arrival of rays with different angles θ. Applying (14) on each monotonicity interval and summing the results, we obtain

$$-\int_{\theta_{\min}(r)}^{\theta_{\max}(r)} t_r(\theta, r)s(\theta, \varphi)\sin\theta\,\mathrm{d}\theta = \sigma(r, \varphi)r. \tag{15}$$

Thus,

$$\int_0^{\pi} K(r, \theta)s(\theta, \varphi)\,\mathrm{d}\theta = \sigma(r, \varphi)r, \qquad r \in [r_{\min}, r_{\max}] \tag{16}$$

where $K(r, \theta) = -\chi(r, \theta)t_r(\theta, r)\sin\theta$,

$$\chi(r, \theta) = \begin{cases} 1 & \text{if} \quad \theta_{\min}(r) < \theta < \theta_{\max}(r), \\ 0 & \text{otherwise.} \end{cases} \tag{17}$$

3.4. Dependence $t(\theta, r)$

In the previous subsection, we found that the kernel $K(r, \theta)$ is determined by the derivative $t_r(\theta, r)$. Unfortunately, this function can be found numerically only.

Numerical analysis shows that $r_t(\theta, t) < 0$ (see figure 5). It means that the function $t = t(r, \theta)$ is uniquely defined on the set

$$\{(r, \theta) \mid \text{there is } t \in [t_{\min}, t_{\max}] \text{ such that } (\theta, t, r) \text{ is an admissible triple}\}. \tag{18}$$

This set has the form $\{(r, \theta) \mid r_1 \leqslant r \leqslant r_2, \theta_{\min}(r) \leqslant \theta \leqslant \theta_{\max}(r)\}$, where the functions $\theta_{\min}(r)$ and $\theta_{\max}(r)$ are shown in figure 7.

To find $t(r, \theta)$, rewrite equations (2)–(6) in a more compact form, excluding the variables s, y, x and δ:

$$G_1 = (R - t)\sin\alpha + \frac{D}{2}\frac{\sin(\alpha - \theta)}{\sin\theta} - R\sin\beta = 0, \tag{19}$$

$$G_2 = r\cos(\alpha - 2\beta) + A\sin(\alpha - 2\beta) \tag{20}$$

$$+ B\frac{n_{\mathrm{q}}\sin(2\alpha - 4\beta)\cos(\alpha - 2\beta)}{2\sqrt{n_0^2 - n_{\mathrm{q}}^2\sin^2(\alpha - 2\beta)}} - R\sin\beta = 0, \tag{21}$$

$$\alpha = \alpha(\theta) = \arccos\left(\frac{n_{\mathrm{w}}}{n_{\mathrm{q}}}\cos\theta\right). \tag{22}$$

The functions $G_j(r, \theta, \alpha, t, \beta)$ constitute a mapping $G : \mathbb{R}^5 \to \mathbb{R}^2$. By the implicit function theorem, this mapping together with the function $\alpha = \alpha(\theta)$ determines the vector function $x(r, \theta) = (t(r, \theta), \beta(r, \theta))$ in a domain, where the partial Jacobian $\left|\frac{\partial G}{\partial x}\right|$, $x = (t, \beta)$, is nonzero.

To find $x(r, \theta)$, for each admissible fixed pair (r, θ), we need to solve the nonlinear system $G(r, \theta, \alpha(\theta), x) = 0$ with respect to x. Then the derivative $t_r(r, \theta)$ entering the kernel of the integral operator is found from the equality

$$x_r(r, \theta) = -(G'_x(r, \theta, \alpha(\theta), x))^{-1}G_r(r, \theta, \alpha(\theta), x), \tag{23}$$

which is obtained from the identity $G(r, \theta, \alpha(\theta), x) = 0$ by differentiation with respect to r. To solve approximately the nonlinear system, we use the Newton–Kantorovich iteration method:

$$x_{n+1} := x_n - (G'_x(r, \theta, \alpha(\theta), x_n))^{-1}G(r, \theta, \alpha(\theta), x_n). \tag{24}$$

The function $t(r, \theta)$ and the kernel of the integral operator found in the indicated way are shown in figure 8.

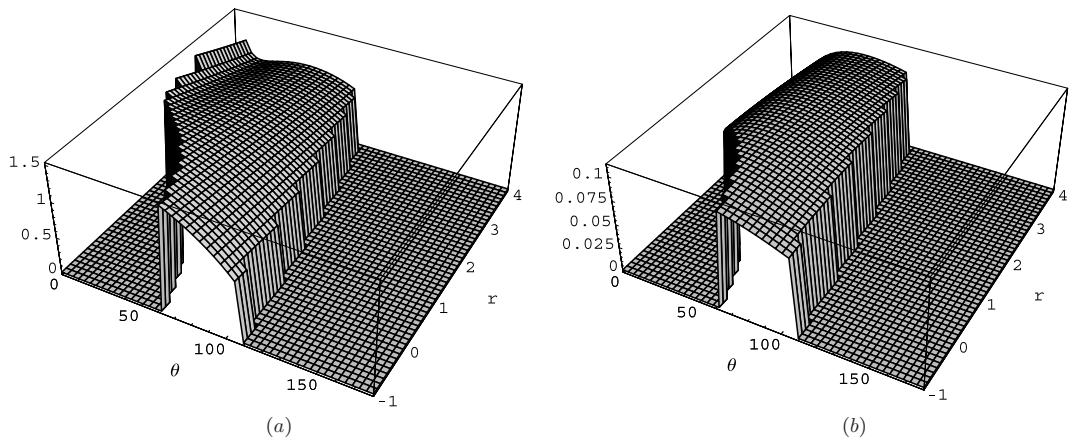

(*a*) (*b*)

Figure 8. The function $t(\theta, r)$ (*a*) and the kernel $K(r, \theta)$ of the operator $\mathscr{K}$ (*b*).

Table 1. Common parameters of experiments.

Wavelength	0.488 μm	Weight w_0	$\exp(5\theta)$
Refractive index of the medium	1.333 (water)	Weight w_1	$\exp(2\theta)$
Refractive index of the particle	1.5	Angle φ	0°
Aspect ratio of the particle	0.5		
The angle between the optical axis and the particle axis	45°		

Table 2. Parameters of particles and reconstruction procedure.

Particle	Figure	Equiv. sphere diameter	Error of the RHS (%)	Parameter α
Disk	10(*a*), 11	2.0	0	10^{-10}
Spheroid	10(*b*)	1.5	0	10^{-10}
Spheroid	10(*c*)	1.5	1	10^{-10}, 10^{-9} (opt), 10^{-8}
Spheroid	10(*d*)	1.5	5	10^{-9}, 10^{-8} (opt), 10^{-7}
Stick	12(*b*)	2.0	0	10^{-10}

3.5. The solution of the integral equation

Since the variable φ plays the role of a parameter in the integral equation (16), we drop it for brevity. Denote the integral operator in (16) by $\mathscr{K}$: $(\mathscr{K}s)(r) = \int_0^\pi K(r,\theta)s(\theta)\,\mathrm{d}\theta$, and agree to consider equation (16) in the space $L_2(0,\pi)$ of square integrable functions. As is well known, the solution of integral operators with piecewise smooth kernels is an ill-posed problem: there is no continuous dependence of the solution on the right-hand side; changing $\sigma(r)r$ with a close function may lead to the situation where a solution does not exist or is nonunique, etc. In practice, the approximate numerical solution of such problems is carried out by various regularization methods.

Apparently, the basic universal method here is the minimization method which consists in the following: an approximate solution s_α to the equation $\mathscr{K}s = \sigma_\delta r$ with an approximate right-hand side $\sigma_\delta r$ given with accuracy δ: $\|\sigma_\delta r - \sigma r\| \leqslant \delta$, is sought by minimization of the functional

$$J_\alpha(s) = \alpha l(s) + \|\mathscr{K}s - \sigma_\delta r\|^2 \tag{25}$$

on some compact subset $M \subset L_2(0,\pi)$, where $\alpha > 0$ is the regularization parameter and $l(s)$ is a convex nonnegative functional on M such that the set $\{s \in M \mid l(s) \leqslant c\}$ is compact for every $c > 0$. It is well known that there is a dependence $\alpha = \alpha(\delta)$ such that the approximate solution $s_{\alpha(\delta)}$ tends to the exact solution as $\delta \to 0$. In practice, the regularization parameter is chosen either empirically or in some other way depending on the error δ of the right-hand side.

If

$$l(s) = \int_0^\pi \left(|s(\theta)|^2 w_0^2(\theta) + |s'(\theta)|^2 w_1^2(\theta)\right)\mathrm{d}\theta, \tag{26}$$

where w_0 and w_1 are some weight functions, then the Euler equation for the minimization problem (25) is

$$\alpha\left(s(\psi)w_0^2(\psi) - s''(\psi)w_1^2(\psi)\right) + \int_0^\pi \left(\int_{r_1}^{r_2} K(r,\psi)K(r,\theta)\mathrm{d}r\right)s(\theta)\,\mathrm{d}\theta = \int_{r_1}^{r_2} K(r,\psi)\sigma_\delta(r)r\,\mathrm{d}r. \tag{27}$$

Discretization of this equation, for example, with the boundary conditions $s'(0) = s'(\pi) = 0$ leads to a system of linear equations with a symmetric positive definite matrix which is solved, for example, by means of the Cholesky decomposition. Detailed information on solving ill-posed problems by the regularization methods can be found in [15–18].

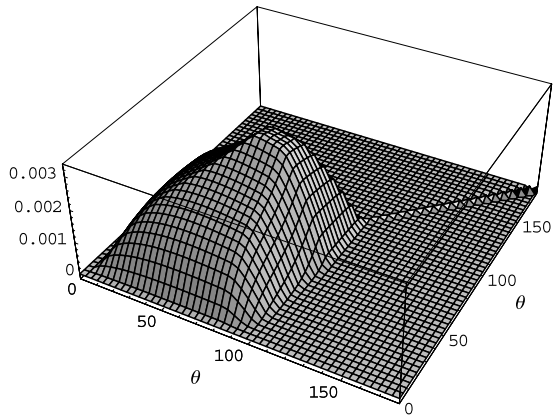

Figure 9. The kernel of the operator $\mathscr{K}^*\mathscr{K}$.

3.6. Choice of the parameters

The parameters $t_{\min}$ and $t_{\max}$ are chosen for the following reasons:

(1) The longer the interval $[t_{\min}, t_{\max}]$, the greater the intensity $\sigma(r)$ and thereby the accuracy with which $\sigma(r)$ is measured. In particular, this is one of the reasons why measuring at a single point t is inefficient. The second reason is given in the next item.

(2) For each fixed t, the set of admissible angles

$$\Theta(t) = \{\theta \mid \exists r \in [r_{\min}, r_{\max}] \text{ such that } (\theta, t, r) \text{ is admissible}\} \tag{28}$$

is sufficiently narrow and does not cover the whole range of angles (see figure 8(*a*)). Moreover, $\Theta(t)$ is broader at large values of t.

(3) On the other hand, increasing $t_{\max}$, we diminish the range of the function $\theta_{\min}(r)$ which is responsible for the disposition of the jump of the kernel K. The presence

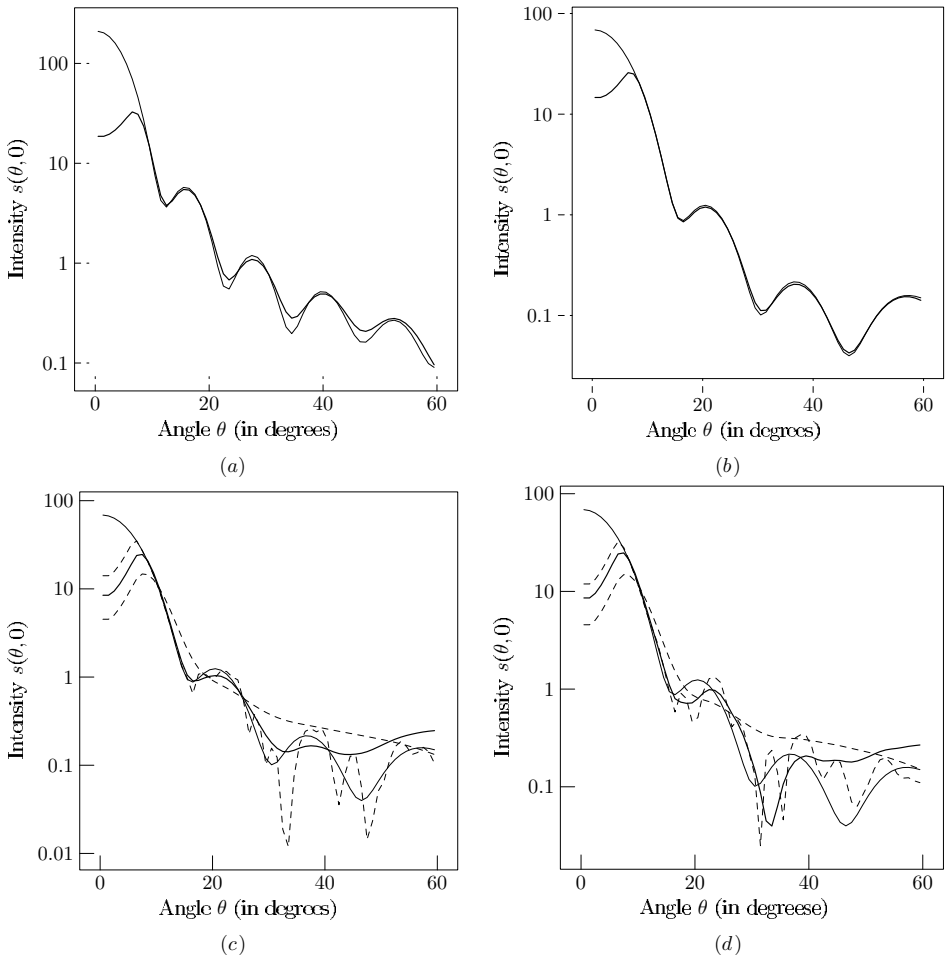

Figure 10. The exact (thin line) and reconstructed 2D LSP's. The optimal reconstructed function is shown by the boldface line; the others are shown by dashed lines.

of this jump makes the solution procedure more stable. Thus, there is no reason to take $t_{\max}$ too large.

(4) In the domain of (r, θ) corresponding to t close to $t_{\min}$ (near the right jump of the kernel in figure 8(*b*)) the kernel $K(r, \theta)$ is rather flat. It means that, although decreasing $t_{\min}$ increases the range of angles, it will hardly lead to stable reconstruction of $s(\theta)$ for these angles.

For the above reasons, in numerics we choose $t_{\min} = 0.8$ and $t_{\max} = 1.5$ for $R = 3$, $A = 2$ and $B = 5$.

In figure 12, we see that the kernel of $\mathcal{K}^*\mathcal{K}$ vanishes for θ greater than some value slightly exceeding $\pi/2$. Therefore, the regularization weights $w_j(\theta)$ should be great for large values of θ. Another reason for this choice is that $s(\theta)$ decays fast in θ.

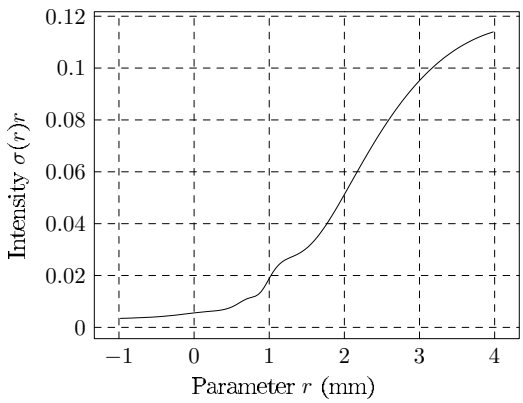

Figure 11. The right-hand side $\sigma(r, 0)r$ for a disk (see figure 10(*a*)).

4. Numerics

The numerical experiment was carried out as follows. Having no real data, we took as the exact solution the entry $S_{11}(\theta, \varphi)$ of the simulated Mueller matrix for various particles and generated the right-hand side $r\sigma(r, \varphi)$ by applying the operator $\mathcal{K}$. The direct scattering problem was solved by the *T*-matrix method code found at http://www.giss.nasa.gov/∼crmim/t_matrix.html (see also [3, 4]). To these model data, we applied our reconstruction procedure and compared the result with the exact solutions. The common and specific parameters of the experiments are given in tables 1 and 2.

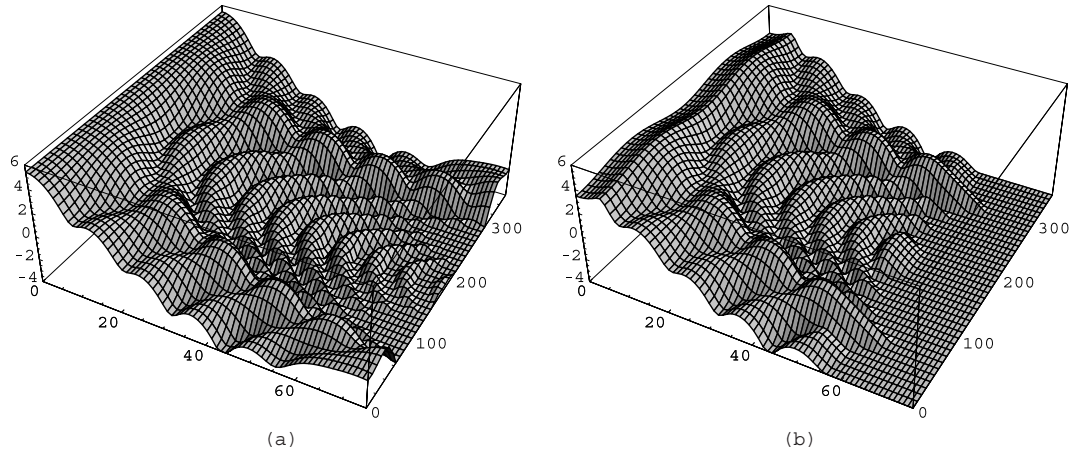

Figure 12. The exact (left) and reconstructed (right) 2D LSP $s(\theta, \varphi)$ for all angles φ. The intensity is shown on a logarithmic scale. (Reconstruction for all $\varphi \in [0, 2\pi]$ is possible only for simulated data.)

Solving the integral equation with the exact right-hand side, we take one small value of α ($\alpha = 10^{-10}$). When the right-hand side is given with some error we take different values of α: for small α the solution is highly oscillating and for large α it is smooth but far from the exact solution. The optimal value of α lies somewhere in between.

5. Conclusion

With this work, we have attempted to modify an optical scheme of the scanning flow cytometer that will allow us to measure the two-dimensional light-scattering pattern of individual particles with a rate up to 500 particles s^{-1}. We have tried to transfer the difficulties caused by complex optical elements from these elements to mathematics. The simulated optical scheme of the SFC was modified by substitution of a widely used CCD camera for the diaphragm-photomultiplier tube unit. The CCD camera should accumulate the scattered light during the time period while the particle is moving within the testing zone of the SFC. The measured two-dimensional plot can be transformed into the two-dimensional light-scattering pattern by means of the developed mathematical inversion procedure. The mathematical inversion allows us to estimate the accuracy of reconstruction of the 2D LSP for non-spherical particles, the influence of the noise on the reconstruction, and to determine the optimal operating angular interval for the current optical scheme of the SFC.

The results introduced in this work give us positive signals to continue modification of the optical scheme of the SFC. As we can see from numerics, if the right-hand side is given exactly then we can expect accurate reconstruction of $s(\theta, \varphi)$ in the range $5^\circ \leqslant \theta \leqslant 50^\circ, 0^\circ \leqslant \varphi \leqslant 180^\circ$ for various types of particles. In the presence of error the accuracy of reconstruction worsens, remaining acceptable for $5^\circ \leqslant \theta \leqslant 20^\circ$.

Following the aim of this research, we would like to provide mathematicians with sufficient experimental data for a successful solution of the inverse light-scattering problem. The solution should open new facilities in individual particle characterization from light scattering forming new diagnostic methods for cell biology. Hematology and immunology are most important fields, where new methods can be effectively applied in the future.

Acknowledgments

The research was financially supported by the Mathematical Sciences Division of the Siberian Branch of the Russian Academy of Sciences (Grant 2006-1.3.1), the Siberian Branch of the Russian Academy of Sciences (Integration Project 2006-03), the Russian Foundation for Basic Research (Grant 07-04-00356), and the State Maintenance Program for the Leading Scientific Schools of the Russian Federation (Grant NSh-7157.2006.1).

References

[1] Bohren C F and Huffman D R 1983 *Absorption and Scattering Light by Small Particles* (New York: Wiley)
[2] Colton D and Kress R 1998 *Inverse Acoustic and Electromagnetic Scattering Theory* (Berlin: Springer)
[3] Mishchenko M I, Travis L D and Lacis A A 2002 *Scattering, Absorption, and Emission of Light by Small Particles* (Cambridge: Cambridge University Press)
[4] Mishchenko M I, Hovenier J W and Travis L D (ed) 2000 *Light Scattering by Nonspherical Particles, Theory, Measurements, and Applications* (San Diego, CA: Academic)
[5] Ramm A G 1992 *Multidimensional Inverse Scattering Problems* (New York: Longman Scientific/Wiley)
[6] Ramm A G 2005 *Wave Scattering by Small Bodies of Arbitrary Shapes* (Singapore: World Scientific)
[7] Maltsev V P and Semyanov K A 2004 *Characterization of Bio-Particles from Light Scattering* (Utrecht: VSP Inverse and Ill-Posed Problems Series)
[8] Chaumet P C, Belkebir K and Sentenac A 2004 *Phys. Rev.* **69** 245405
[9] Zakovic S, Ulanowski Z J and Bartholomew-Biggs M C 1998 *Inverse Problems* **14** 1053

[10] Kachel V, Fellner-Feldegg H and Menke E 1990 *Flow Cytometry and Sorting* ed M R Melamed, T Lindmo and M L Mendelsohn (New York: Wiley) pp 27–45
[11] Kaye P H, Aptowicz K, Chang R K, Foot V and Videen G 2007 *Optics of Biological Particles* ed A Hoekstra, V Maltsev and G Videen (Dordrecht: Springer) pp 31–61
[12] Neukammer J, Gohlke C, Hope A, Wessel T and Rinneberg H 2003 *Appl. Opt.* **42** 6388
[13] Chernyshev A V, Prots V I, Doroshkin A A and Maltsev V P 1995 *Appl. Opt.* **34** 6301–5
[14] Maltsev V P 2000 *Rev. Sci. Instrum.* **71** 243–55
[15] Isakov V 2006 *Inverse Problems for Partial Differential Equations* (Berlin: Springer)
[16] Ivanov V K, Vasin V V and Tanana V P 2002 *Theory of Linear Ill-Posed Problems and Its Applications* (Leiden: Brill Academic)
[17] Lavrentev M M, Romanov V G and Shishatskiĭ S P 1986 *Ill-Posed Problems of Mathematical Physics and Analysis* (Providence, RI: American Mathematical Society)
[18] Tikhonov A N and Arsenin V A 1977 *Solutions of Ill-posed Problems* (Washington, DC: Winston & Sons)